Journal of Power Sources 196 (2011) 3141–3148

Contents lists available at ScienceDirect

Journal of Power Sources

journal homepage: www.elsevier.com/locate/jpowsour

Design of thermal management subsystem for a 5 kW polymer electrolyte membrane fuel cell system

Saeed Asghari*, Hooman Akhgar, Bagher Faghih Imani

Engineering Research Institute, Isfahan Engineering Research Center, 7th kilometer of Imam Khomeini Ave., P.O. Box 81395-619, Isfahan, Iran

ARTICLE INFO

Article history:
Received 9 June 2010
Received in revised form
10 November 2010
Accepted 18 November 2010
Available online 24 November 2010

Keywords:
Polymer electrolyte membrane fuel cell
Thermal management subsystem
Cooling flow field
Parallel serpentine pattern

ABSTRACT

High-efficiency thermal management subsystem has a key role on the PEM fuel cell performance and durability. In this study, design of thermal management subsystem for a 5 kW PEM fuel cell system is investigated. A numerical model is presented to study the cooling flow field performance. The number of parallel channels in parallel serpentine flow field is selected as the design parameter of the flow field and its optimum value is obtained by compromising between the minimum pressure drop of coolant across the flow field and maximum temperature uniformity within the bipolar plate criteria. The optimum coolant flow rate is also determined by compromising between different criteria. Test results of a 5-cells short stack are presented to verify the numerical simulation results.

1. Introduction

There are several technical challenges for the polymer electrolyte membrane fuel cell (PEMFC) technology to be commercialized. Among them, the proper thermal management has been recognized as one of the most critical issues. Improper thermal management causes electrolyte drying (global or local) or electrode flooding which both lower the fuel cell performance. In the case of global drying, the output voltage decreases, and consequently the electrical efficiency decreases. In the local drying case, the ohmic resistance of membrane increases in the dried region which generates more heat in turn. This additional heat causes the membrane to become more dried out locally. This unstable process continues until hot points form in the membrane electrode assembly (MEA), and finally local MEA failure occurs.

Low temperature PEM fuel cells work in the temperature range of 60–80 °C and can tolerate only small temperature variations [1]. These temperature restrictions come from the properties of the electrolyte material. As the polymer electrolyte must be sufficiently hydrated to conduct the protons efficiently, so the maximum working temperature should not exceed 80 °C; because, the water absorption tendency of inlet reactant gases increases as the working temperature rises which results in the electrolyte drying. On the other hand, working on low temperature may lead to water condensation and flooding of electrodes, which results in voltage loss due to increased resistance to reactants mass transport. Working on the temperatures lower than 60 °C also results in lower reaction rates and consequently lower efficiency and output electrical power.

A PEM fuel cell produces an amount of heat close to its electrical power at its nominal working voltages e.g. 0.6 V per each cell. Heat generation in PEMFC is resulted from four factors: entropic heat of reactions, irreversibility of electrochemical reactions, ohmic resistances and water condensation [1–3]. The entropic heat is a representation of the entropy change of the electrochemical reaction and must be supplied to or removed from the electrode compartment. The irreversibility of the electrochemical reactions inside a fuel cell is a significant source of heat generation. The ohmic heat is resulted from both the proton current in the electrolyte and the electron current in the electrodes and bipolar plates as well as current collectors.

There are some ways to remove the generated heat from a fuel cell stack:

- Free convection from edges to surrounding.
- Phase change of coolant media.
- Air cooling.
- Water cooling.

Decision of cooling method for a fuel cell stack depends on the factors such as: fuel cell power, complexity, cost, recovering of heat e.g. in a combined heat and power system (CHP). The first cooling

* Corresponding author at: Isfahan Engineering Research Center, 7th kilometer of Imam Khomeini Ave., Isfahan, Iran, P.O. Box 81395-619. Tel.: +98 311 3222428; fax: +98 311 3222446.
E-mail address: asghari@fuelcell.ir (S. Asghari).

0378-7753/$ – see front matter © 2010 Elsevier B.V. All rights reserved.
doi:10.1016/j.jpowsour.2010.11.077

Nomenclature

g	acceleration of gravity ($m\,s^{-2}$)
Gr	Grashof number
h	convective heat transfer coefficient ($W\,m^{-2}\,°C^{-1}$)
I	stack current (A)
k	thermal conductivity of ambient air ($W\,m^{-1}\,K^{-1}$)
L	characteristic length (m)
N	number of cells in stack
Nu	Nusselt number
Pr	Prandtl number
Q	heat generation (W)
Ra	Rayleigh number
T_∞	ambient temperature (°C)
T_s	surface temperature of bipolar edge (°C)
T_f	film temperature (°C)
V	cell voltage (V)

Greek symbols

β	volumetric thermal expansion coefficient ($°C^{-1}$)

Subscript

i	cell number

method is mainly used for fuel cells up to 100 W of output electrical power. The second method is an initiative method and has not been used as a practical solution for heat removal from a fuel cell stack. Air cooling and water cooling are more conventional methods for fuel cell stack cooling. As a rule of thumb, PEM fuel cell stacks above 5 kW should be water cooled, those below 2 kW air cooled, with a decision for stacks in between being a matter of judgment [4,5]. Essentially, air cooling method is simpler and needs fewer accessories but has some disadvantages. As the output power increases, it becomes harder to maintain a uniform temperature distribution within the stack by the air cooling method and the parasitic losses related to cooling fan increase inevitably. Because the specific heat of air is low and as a result, much air is needed to remove the generated heat. In addition, the dimensions of air cooling channels should be larger than those of water cooling channels, which make the stack larger than it needs to be. On the other hand, temperature distribution within the stack could be more uniform and the heat removal would be more efficient by using water cooling method; however, this method needs more accessories and severe control schemes.

A number of studies of fuel cells have been conducted to investigate heat and mass transfer issues in the PEM fuel cells [6–9]. A few papers have been published in the field of analyzing, designing and optimizing the thermal management subsystem of a PEM fuel cell. Chen et al. [10] conducted a cooling flow field design and optimization process using computational fluid dynamic (CFD) method. They concluded that modified serpentine flow field has the most temperature uniformity within the bipolar plate among proposed different serpentine and parallel types. Nevertheless, they did not consider the role of thermal management subsystem on the cooling flow field design and optimization. Musser and Wang [11] employed a two-dimensional code to predict the temperature variation in the fuel cell. Zhang et al. [12] developed a model for thermal behavior of thermal management subsystem including stack, radiator, pump, fan, which enables the variation of the temperature of the PEMFC stack as well as the other components of the thermal management subsystem. Their model predicted that the thermal efficiency increases with an increase of air flow rate, decreases with an increase of cooling water flow rate, and decreases slightly with an increase of environment temperature. Adzakpa et al. [13] developed a 3D dynamic thermal model for a single cell to study the temperature distribution within a fuel cell cooled from the bottom to the top with air. The model was governed by the thermal energy balance taking into account the inlet gas humidity. They concluded that the cell temperature is directly linked to the current density and the gas humidity. Yu and Jung [14] developed a thermal model of PEM fuel cell and a thermal management subsystem to investigate the design criteria of thermal management and to develop a thermal management strategy for fuel cells with large active cell areas.

In this research, design of cooling flow field for a 5 kW PEMFC system is investigated. Optimum working conditions of thermal management subsystem are also determined using numerical simulation and experimental results. The results of the numerical simulation are verified by some experimental tests.

2. Experimental

A single cell was designed and manufactured to extract the polarization curve of the selected MEA for using in the stack under different working conditions. The resultant polarization curve was used as the input parameter for the coolant flow field design process.

A short stack consisted of 5 cells with the same anode and cathode flow fields and MEA as those of the single cell, was also designed and manufactured using final designed cooling flow field in order to verify the simulation results as well as the suitability and effectiveness of the designed cooling flow field.

The MEA with an active area of 225 cm^2 consisted of NRE-211 membrane, catalyst layers with a total Pt loading of 0.4 mg cm^{-2} at both the anode and the cathode sides and SGL carbon cloth with microporous layer as the gas diffusion layer (GDL). The anode and the cathode flow fields were of parallel serpentine pattern. The cross-section of the flow channels were 1 mm × 1 mm at both the anode and the cathode sides.

After cell stack assembly, a break-in period is necessary to test and condition the MEAs and other assembled components in order to get the fuel cell to achieve peak performance and consistent current output at a specific voltage. It is theorized that the electrodes, ionomers within the electrodes and the PEM electrolyte are slowly hydrated during the break-in period. By being fully hydrated, ionic resistance of the MEA is reduced and the effective surface areas of the catalysts available for fuel cell electrochemical reactions are increased, thereby enhancing performance of the fuel cell [15]. The MEAs were broken-in prior to carrying out the tests. The experiments were conducted using a homemade 1 kW test station. Hydrogen and air were discharged at a constant stoichiometry of 1.5 and 2.5, respectively and the relative humidity of 95%. Operating pressures of the anode and the cathode were kept constant at 1.1 bar (g) and 1.0 bar (g), respectively. Operating temperatures of the single cell as well as the short stack were kept constant at 60 °C, unless otherwise stated.

In a thermal management subsystem of a PEM fuel cell system, cooling fluid passes through heat exchanger, bypass valve, water management system (in PEM fuel cell systems which have coupled thermal and water management subsystems), rotameter, etc., besides the fuel cell stack which all of them have their own flow rate–pressure drop characteristic. A thermal management subsystem which is shown schematically in Fig. 1, was also designed and developed for the 5 kW PEMFC system. This subsystem, combined with the 5-cells short stack, was used to extract flow rate–pressure drop characteristic of the subsystem components and also to determine the optimal operating parameters of the subsystem like optimum coolant flow rate.

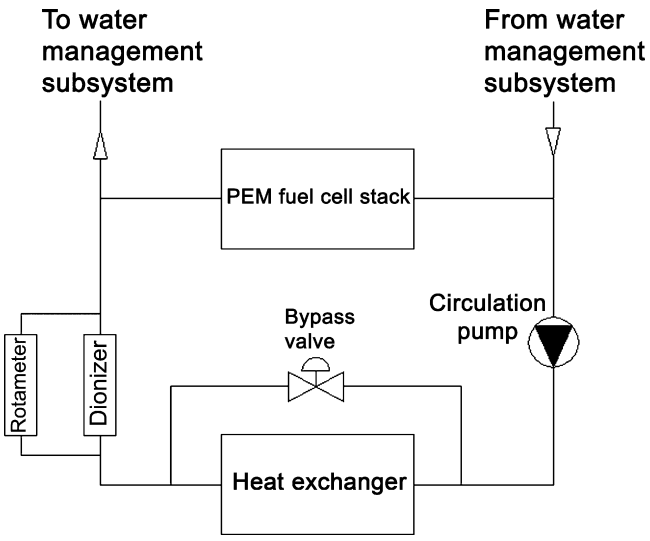

Fig. 1. A schematic view of the thermal management subsystem for 5 kW PEM fuel cell system.

Fig. 2. Temperature measurement of the bipolar plate edges by the infrared thermometer.

A series of temperature measurement tests were carried out on the short stack to verify the numerical simulation results. Since determination of temperature distribution within the bipolar plates was impossible during fuel cell stack operation, it was decided to measure the temperature distribution along bipolar plate edges instead. The temperature measurements were made along the vertical and horizontal edges of the bipolar plates of third cell in the short stack. An especial test setup (Fig. 2) was developed to carry out the temperature measurement. A tape with equally spaced punched holes was attached to the bipolar plate edges and surface temperature at the center of these holes was measured by a CHY infrared thermometer (model: CHY 111A).

3. Numerical simulation

3.1. Extraction of input parameters

Polarization curve of the MEA is the key input parameter of the simulation because the amount of heat generation at any working voltage can be calculated easily using this curve. The single cell which employed the same MEA as that had been considered for using in the stack, was tested under different working temperatures to investigate the effect of operating temperature variations on the polarization curve and also to find the optimum working temperature of the cell. Operating temperature of the single cell was ramped up from room temperature to a point where no considerable improvement was observed. Fig. 3 shows the polarization curves of the single cell at different operating temperatures. As this figure shows, the performance of the single cell improves as the operating temperature increases; however, the rate of performance enhancement with temperature decreases as the temperature increases i.e. working on the temperatures higher than 60 °C has no considerable effect on the performance improvement. On the other hand, working on higher temperatures has a risk of formation of local hot points in the cell active area which may lead to MEA failure. Therefore, the temperature of 60 °C is chosen as the operating temperature of the stack and its related polarization curve is selected as the input parameter of the numerical simulation. The heat generation per each cell in the stack at any working voltage per cell can now be determined by using of this polarization curve as [4]:

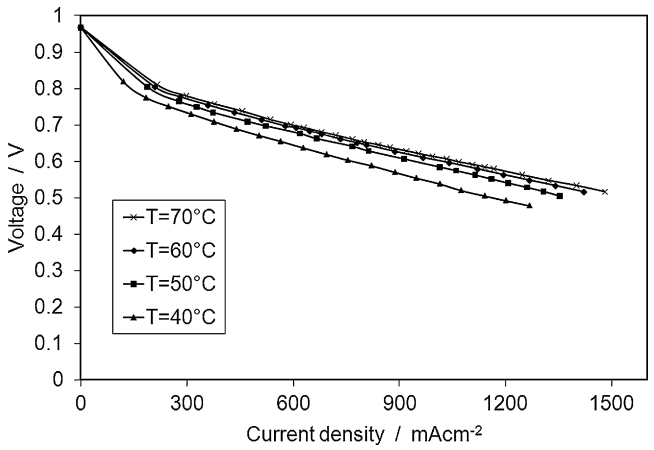

Fig. 3. Polarization curves of the single cell at different working temperatures. Stoichiometry: 1.5/2.5 for H_2/air; RH: 95/95% for H_2/air; pressure: 1.1/1.0 bar (g) for anode/cathode.

$$Q_i = (1.23 - V_i)I \tag{1}$$

where Q_i, V_i and I denote heat generation per cell, working voltage of the cell and output electrical current of the stack, respectively. The voltage of $V_i = 0.6$ V is selected as the nominal voltage per each cell in the stack.

It is expected that most of the generated heat in a fuel cell stack will be removed by the coolant; however, some smaller portions of the heat may be removed by free convection from stack faces to surrounding and also by the reactants exiting from the stack. The free convection from bipolar plate edges to surrounding is included in the numerical model to investigate the effect of heat removal by the free convection. Heat convection coefficients are separately determined for vertical and horizontal edges by governing relations 2–7 from Incropera and DeWitt [16]:

$$h = \frac{Nu_l k}{L} \tag{2}$$

$$Nu_l = 0.68 + \left[\frac{0.67\,Ra^{1/4}}{(1 + (0.492/Pr)^{9/16})^{4/9}}\right] \tag{3}$$

$$Ra = Gr\,Pr \tag{4}$$

$$Gr = \frac{g\beta(T_s - T_\infty)L^3}{\vartheta^2} \tag{5}$$

$$\beta = \frac{1}{T_f} \quad (6)$$

$$T_f = \frac{T_s - T_\infty}{2} \quad (7)$$

According to the criteria mentioned in Section 1, water cooling method is used for the 5 kW system and de-ionized water is selected as the coolant.

It is assumed that the MEAs in the stack have the same performance as when they are used in the single cell alone; however, some reduction in MEA performance is probable when used in the stack.

3.2. Geometric model

Cooling flow field and related inlet and outlet manifolds should be designed in such a way that the following requirements are fulfilled simultaneously:

1 *Removing generated heat at different working voltages*: the thermal output power of the fuel cell stack varies as its electrical output power varies, i.e. the generated heat increases as the electrical output current of the stack increases. Since the fuel cell stack may operate under different working voltages, so cooling flow field should be designed in such a way that it removes generated heat at large range of working voltages.
2 *Minimum pressure drop across flow field from the inlet to the outlet*: power consumption of the circulation pump of thermal management subsystem increases as the pressure drop across the flow field increases which results in decreasing net electrical output power of the fuel cell system. Therefore, cooling flow field should be designed in such a way that the pressure drop from the inlet to the outlet be as low as possible.
3 *Uniform temperature distribution*: Since the rate of cell reactions and also current density at a working voltage depend on the temperature besides the other factors, so the temperature distribution within the cell active area should be uniform in order to obtain uniform cell reaction rate and current density within the cell active area. Non-uniform current density distribution may lead to some MEA damage. Hence, maintaining uniform temperature distribution within the cell active area is one of the key roles of the cooling flow field.

Different types of cooling flow fields can be considered for water cooled PEMFC stacks. Among different types, serpentine, parallel and parallel serpentine are the most conventionally used types. The parallel serpentine type cooling flow field requires smaller coolant flow rate than the parallel type to maintain uniform temperature distribution within the fuel cell stack; however, coolant pressure drop from the inlet to the outlet associated with the serpentine type flow field is higher than that of the parallel type [10]. Regarding to its advantages, the parallel serpentine type is selected as the coolant flow field.

In the manufacturing phase of the fuel cell stack, only one half of the cooling flow field is machined in each bipolar plate and when the stack is assembled, the bipolar plates of the two adjacent cells come into contact and form the entire cooling flow field existing between these two cells. The separation plane of two adjacent bipolar plates related to two adjacent cells, which halves the cooling flow field is a symmetry plane and characterized here as x–y plane (Fig. 4). In addition, the half of the cooling flow field in each bipolar plate has symmetry with respect to median line along x-axis (Fig. 4). Only one-fourth of the cooling flow field is indicated in Fig. 4; however, contour plots of temperature and pressure distributions are plotted for the whole of the flow field by mirroring, in the subsequent sections.

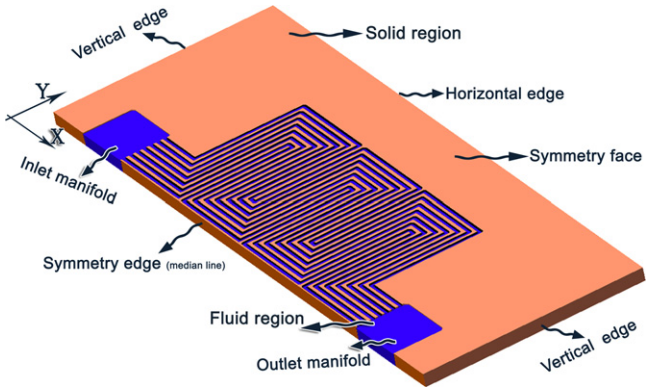

Fig. 4. The geometric model developed for the numerical simulation. Different regions, boundary conditions, and symmetry boundary conditions are indicated.

The geometric model is composed of two regions: solid region (bipolar plate) and the fluid region (coolant). Solid region is assumed to be carbon-loaded composite with the thermal conductivity of 12.2 W m^{-1} K^{-1}. Free convection to surrounding from bipolar plate edges and heat flux continuity at the coolant–bipolar plate interface are the thermal boundary conditions of the solid region. Constant and uniform heat flux boundary condition is imposed on the opposite side of the bipolar plate (the side which is in contact with the MEA) to incorporate the generated heat from the cell reactions into the model. The heat flux is calculated by dividing the generated heat by the active area of the fuel cell. Here, a simplification is made by assuming that the heat flux resulted from cell reactions to be uniform over the active area; however, heat flux distribution may not be so uniform in real conditions. Heat flux distribution depends on some primary and secondary factors like uniformity of reactants distribution over the cell active area, uniformity of assembly pressure distribution between cell components, uniformity of catalyst coating on the membrane, etc. Cathode and anode flow fields have critical roles on the output current density and the generated heat flux uniformities. In the designing process of the cathode and anode flow fields, it was tried to design these flow fields in such a way that the resultant current density and generated heat flux be uniform as much as possible.

The material of the fluid region is assumed to be de-ionized water with temperature dependent physical properties. It is assumed that the coolant enters the flow field at the constant temperature of 60 °C. Inlet and outlet boundary conditions of the fluid region are assumed to be mass flow inlet and pressure outlet, respectively.

Due to symmetry of the geometrical model with respect to x–y plane as well as the median line along x direction, only one-fourth of the final flow field is modeled and simulated (Fig. 4). Regarding the thickness of the bipolar plate and space limitations, cross-section of the coolant flow channels is selected to be 2 mm × 5 mm.

The solid and the fluid regions of the model composed of 132,3931 and 20,0809 hexahedral cells, respectively.

4. Results and discussion

The numerical model was run under different coolant flow rates. Contour plots of temperature distribution within the coolant and the bipolar plate at the working voltage per cell of 0.6 V and the coolant flow rate per cell of 0.48 liter per minute (LPM), are shown in Figs. 5 and 6, respectively. It can be seen from Fig. 5 that the temperature increase along the channels is uniform over all of the channels and the total temperature increase from the inlet to the outlet is about 1.8 °C. As Fig. 6 shows, the maximum temperature difference within the bipolar plate is about 7.4 °C. There are four

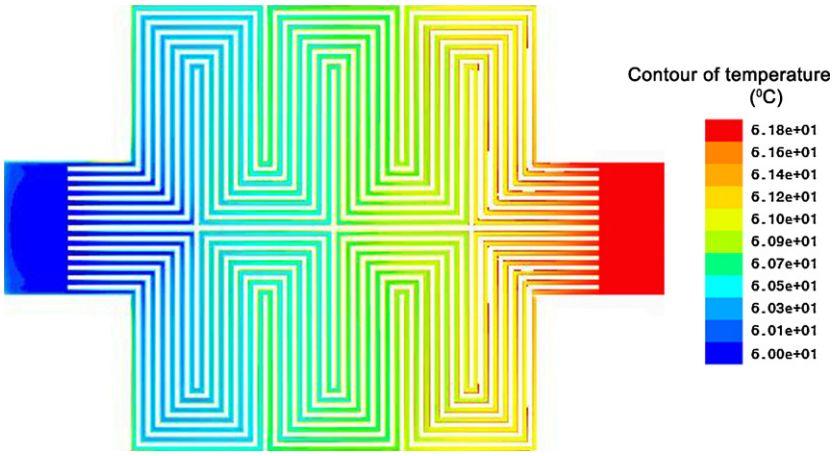

Fig. 5. Contour plot of temperature distribution within the coolant at the coolant flow rate of 0.48 LPM.

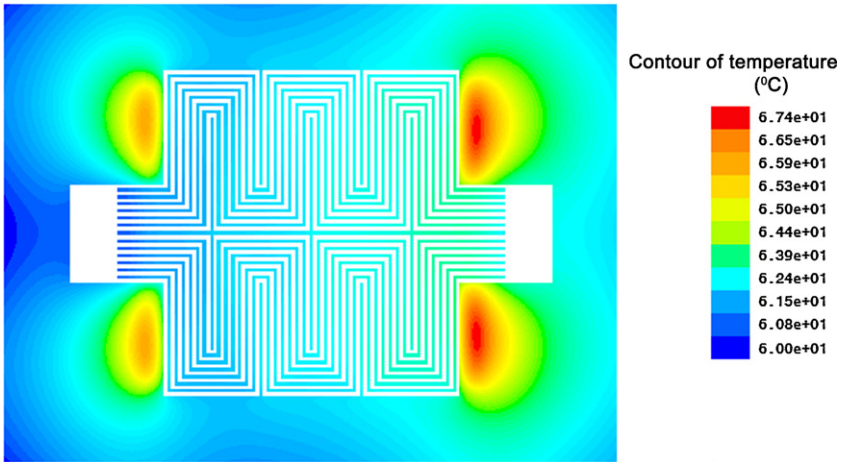

Fig. 6. Contour plot of temperature distribution within the bipolar plate at the coolant flow rate of 0.48 LPM.

temperature concentration points near the corners of the flow field. The reason may be due to the larger cell active area compared to the area that the coolant flow field covers. Space and physical limitations urge the cooling flow field area to be lower than the cell active area. Therefore, it is better to insert the inlet and the outlet manifolds of the reactant gases in these points in order to reduce the temperature concentration and also obtain more temperature uniformity.

Pressure distribution contour plot of the coolant at the flow rate of 0.48 LPM is shown in Fig. 7. As this figure shows, there is a pressure drop of about 700 Pa between the inlet and outlet of the flow field. The pressure drop is uniform over different channels; therefore, the cooling channels deliver the same value of the coolant. Because, the value of delivered coolant flow rate to each channel is a direct function of coolant pressure drop along the channel. In addition, trends of the coolant temperature increase along different channels are the same which is an indication of uniform coolant distribution between different channels.

4.1. Determination of number of parallel channels

The number of parallel channels in the parallel serpentine flow field may be considered as a design variable. Different parallel serpentine patterns with different numbers of parallel channels were considered for the cooling flow field and simulated in order to choose the optimum number of parallel channels. Variations of coolant pressure drop between the inlet and outlet of the flow field and temperature difference between the exit coolant and the bipolar plate as a function of number of parallel channels are indicated in Fig. 8. As seen from this figure, the pressure drop decreases as the number of parallel channels increases. This is due to the fact that the lengths of channels as well as the amount of coolant delivered to each channel which both directly influence the pressure drop, are decreased by increasing the number of parallel channels. On the other hand, the temperature difference between the exit coolant and the bipolar plate increases as the number of parallel channels increases. Because of space limitations, the area covered by the cooling flow field decreases as the number of parallel channels increases which leads to more increased nonuniform temperature distribution within the bipolar plate, specially at the exit region. Since the outlet temperature of the coolant is considered to be independent of the number of channels, so the temperature difference between the exit coolant and the bipolar plate increases at the exit region. In addition, the rate of variations decreases as the number of parallel channels increases. According to discussion above, it is desirable to increase the number of parallel channels in the viewpoint of lower pressure drop criteria; however, this increase is not suitable in the viewpoint of temperature uniformity. It is decided that the cooling flow field comprises 14 channels in parallel because the temperature difference of 5.5 °C between the exit coolant and the bipolar plate is located in our desirable range.

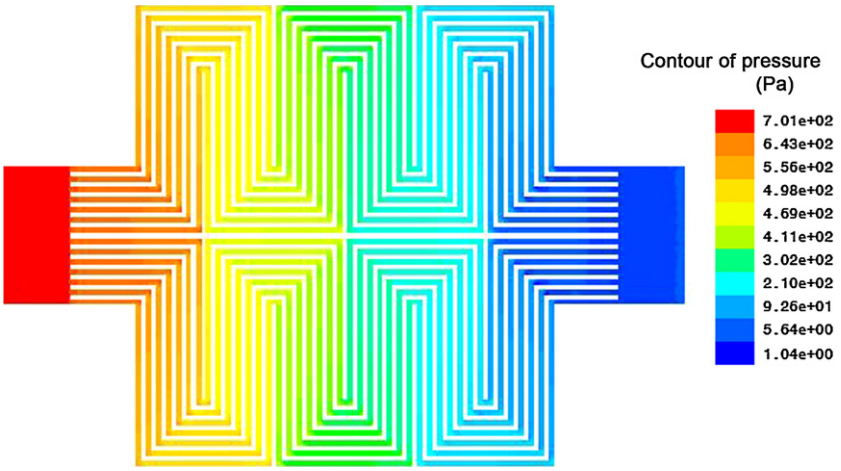

Fig. 7. Contour plot of pressure distribution within the coolant at the coolant flow rate of 0.48 LPM.

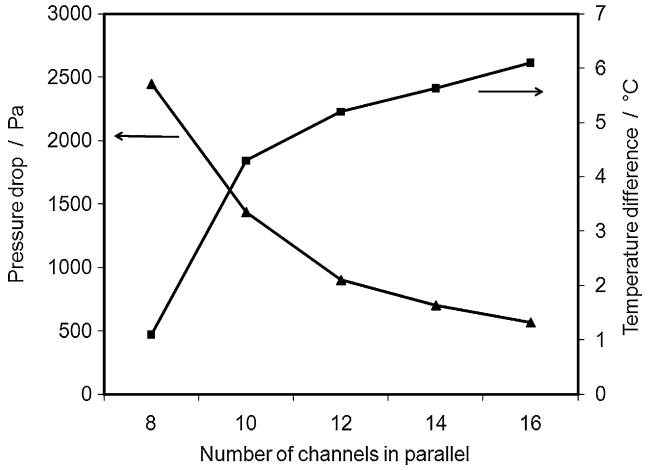

Fig. 8. Effect of number of parallel channels in the parallel serpentine flow pattern on the coolant pressure drop from inlet to the outlet of the flow field and temperature difference between the exit coolant and the bipolar plate at the coolant flow rate of 0.48 LPM.

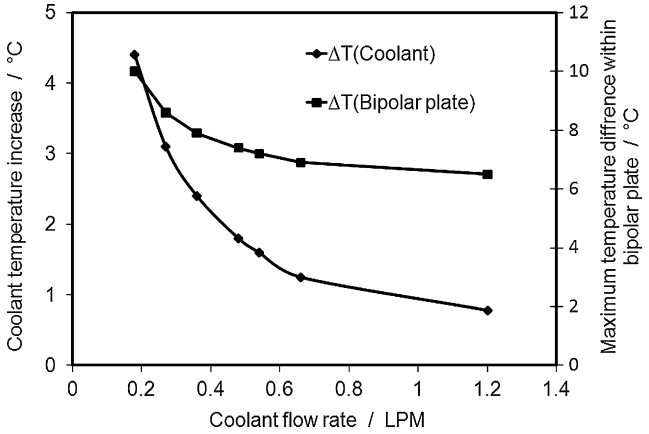

Fig. 9. Coolant temperature increment and maximum temperature difference within the bipolar plate versus coolant flow rate per cell.

4.2. Determination of optimum coolant flow rate

The optimal coolant flow rate for each cell in a fuel cell stack is another design variable of thermal management subsystem of a PEMFC system. Fig. 9 shows the coolant temperature increase from the inlet to the outlet and maximum temperature difference within the bipolar plate as a function of coolant flow rate at the working voltage of 0.6 V per cell for the parallel serpentine flow field having 14 channels in parallel. As expected, the values of both parameters decrease by increasing the coolant flow rate; however, the rate of decrease at lower flow rates is larger than that of higher flow rates. Hence, regarding to uniform temperature distribution criteria, it is beneficial to increase the coolant flow rate as much as possible, but as Fig. 9 shows, increasing coolant flow rate to the values higher than 0.48 LPM may not have any considerable effect on the temperature uniformity. For example, increasing the coolant flow rate by 0.7 LPM results in only 0.8 °C decrease of maximum temperature difference.

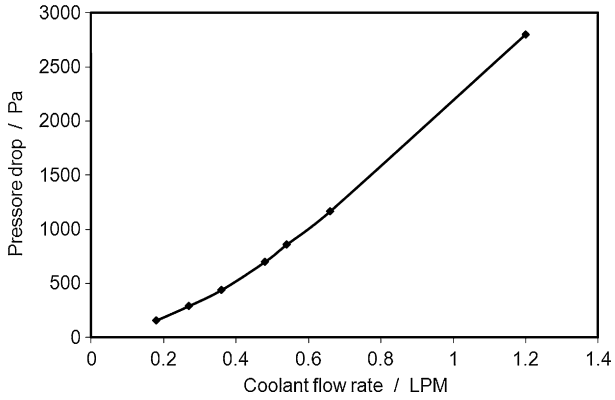

Fig. 10. Coolant pressure drop across the cooling flow field versus the coolant flow rate.

Fig. 10 shows the relationship between coolant pressure drop across the flow field and its flow rate. As this figure shows, the pressure drop and the parasitic losses related to the coolant circulation pump increases progressively as the coolant flow rate increases. The relationship between the pressure drop and the flow rate is nearly linear; however, second order terms come from channel bendings influence the pressure drop but their values are negligible in comparison to the linear term coming from friction losses. Regarding to minimum pressure drop criteria, it is desirable to reduce the coolant flow rate as low as possible. Higher coolant flow rate causes more uniform temperature distribution within the bipolar plate (Fig. 9); while lower flow rate leads to lower pressure drop and parasitic losses (Fig. 10). Hence, the trends of pressure drop and temperature uniformity variation with respect to the coolant flow rate are contrary to each other; therefore, optimum

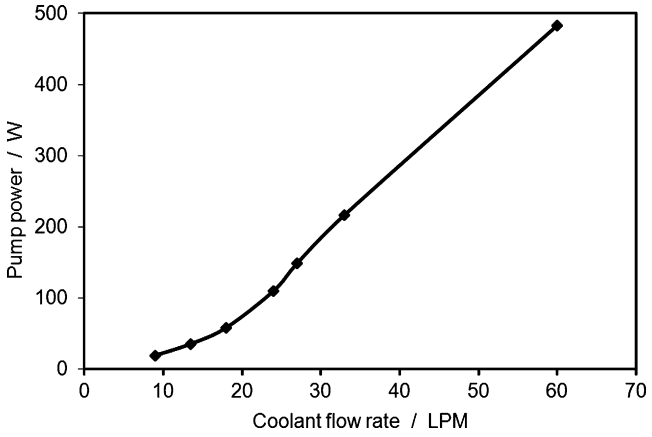

Fig. 11. Power consumption of the circulation pump versus coolant flow rate of 5 kW PEM fuel cell system.

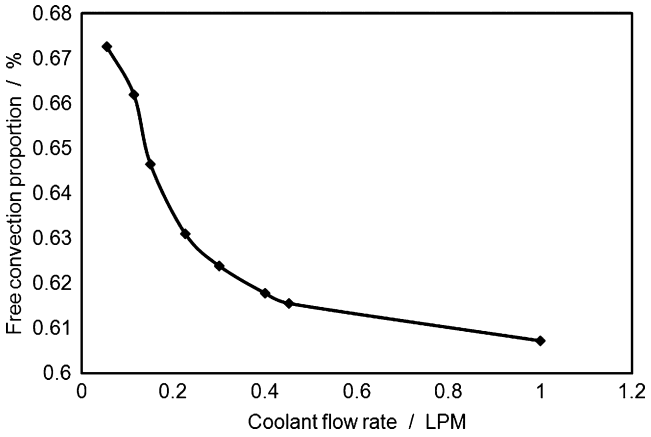

Fig. 12. Proportion of the free convection heat removal from bipolar edges to the total generated heat versus coolant flow rate per cell.

coolant flow rate should be determined in a manner that a compromise between maximum temperature uniformity and minimum pressure drop criteria be achieved.

Required power of the coolant circulation pump is another parameter that has a key role in determining optimum coolant flow rate because the net electrical output power of the fuel cell system decreases as the power consumption of the circulation pump increases. The required power of the circulation pump can be computed by determining the flow rate–pressure drop characteristics of the coolant flow field and components of thermal management subsystem. The pressure drop–flow rate characteristics of the subsystem components were obtained experimentally by the developed thermal management subsystem for the 5 kW fuel cell system (Fig. 1). Required power of the circulation pump was computed at different flow rates by considering a specified efficiency for the circulation motor-pump. Fig. 11 shows the required power of the circulation pump as a function of flow rate for a 5 kW system which contains a 50-cells stack. As this figure shows, the required power is relatively small at the flow rates lower than 24 LPM, but increases abruptly after that. By referring to Fig. 9, it reveals that the coolant temperature increment across the flow field and the maximum temperature difference within the bipolar plate at the average coolant flow rate per cell of 0.48 LPM, which corresponds to 24 LPM for 50-cells stack, are 1.8 °C and 7.4 °C, respectively. These values are located in our desirable range. Hence, the flow rate of 24 LPM is selected as the optimum coolant flow rate for 50-cells stack at the nominal working voltage of 0.6 V per cell. It should be noted that the value of optimal flow rate depends on the type and performance of the membrane electrode assembly, pattern of cooling flow field and the size of the cell (cell active area). Therefore, the optimal flow rate may vary from the value obtained in the present research as the type or size of the MEA and/or pattern of cooling flow field change. For example, the nonuniformity of temperature distribution within the bipolar plate may increase as the cell active area increases; therefore, more coolant flow rate is needed to maintain the maximum temperature difference within the bipolar plate in a specified range. Hence, the optimal flow rate may increase as the cell active area increases.

4.3. Free convection from stack faces

As mentioned earlier, the free convection from stack surfaces was also implemented into the numerical model to account for its role on the heat removal. Fig. 12 shows the proportion of the free convection heat removal from stack faces to the total generated heat versus the coolant flow rate per cell. As this figure shows, this proportion decreases by increasing the coolant flow rate; however, the value of heat which is removed by free convection is negligible compared to the value of heat which is removed by the coolant. Hence, free convection to surrounding from bipolar edges can be ignored in thermal modeling without any considerable effect on the simulation results.

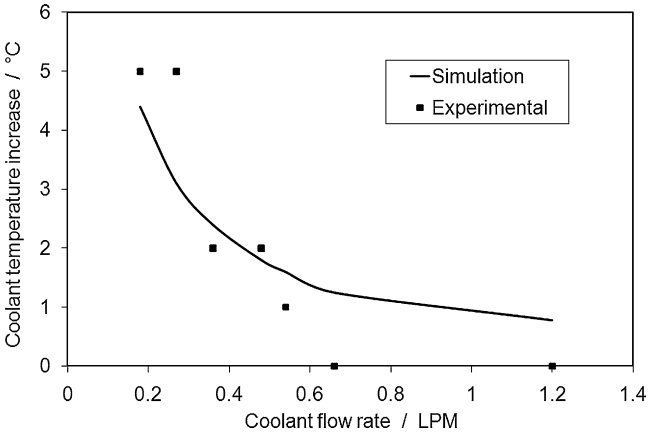

Fig. 13. Coolant temperature increment from inlet to the outlet versus coolant flow rate per cell in the 5-cells short stack.

4.4. Verification of simulation results

The 5-cells short stack and the developed thermal management subsystem were assembled and put under different test in order to verify the simulation results. A series of temperature measurement at the same nominal working conditions but different coolant flow rates were carried out on the 5-cells short stack in order to verify the simulation results. In each test, the coolant flow rate was regulated in such a way that each cell delivered flow rate equal to the value assumed in the simulation.

Temperature increments of the coolant at different flow rates obtained from experimental measurements are compared to those obtained by the numerical simulation in Fig. 13. Coolant flow rates in the figure are related to the average flow rate delivered to each cell, which is simply determined by dividing the total flow rate by the number of cells (5 cells). As seen from this figure, there is a good agreement between the simulation and the experimental results. The experimentally measured temperature rises at the coolant flow rates of 0.66 LPM and 1.2 LPM are equal to zero. This is due to the fact that the thermocouples which had been assembled in the inlet and outlet ports did not have decimal precision.

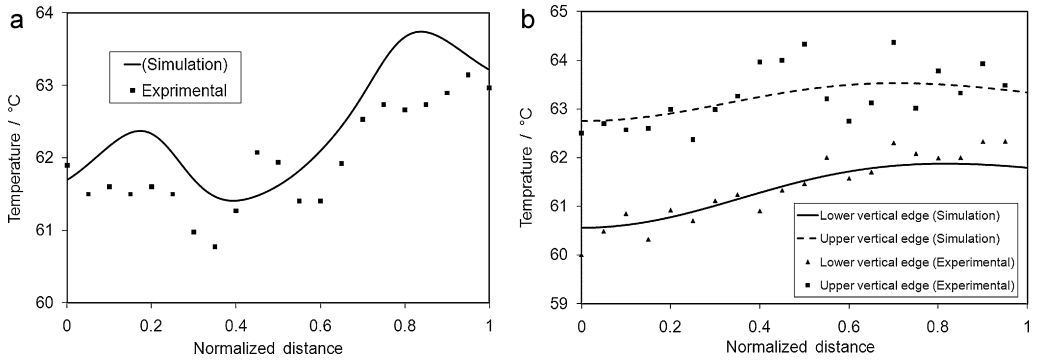

Fig. 14. Temperature profiles along (a) horizontal edge and (b) vertical edges of the 4th bipolar plate of the 5-cells short stack at the average coolant flow rate of 0.48 LPM per cell during 5-cells short stack testing. Upper vertical edge and lower vertical edge stand for the vertical edges near to the inlet and outlet coolant manifolds, respectively.

As mentioned in Section 2, a series of temperature measurement was carried out along the bipolar plate edges. Temperature variations along the horizontal edge of the 4th bipolar plate in the short stack obtained from the simulation and experiments at the nominal working conditions are compared to each other in Fig. 14a. A good agreement between the numerical simulation and the experimental results can be observed. The temperature increases by moving from the vertical edge to the median line of the bipolar plate. Therefore, point of maximum temperature along the horizontal line is located on the vertical symmetry line of the bipolar plate. It is also revealed from this figure that the simulation results predict two peaks at the normalized distances of 0.2 and 0.82 while these peaks are not experimentally observed during the tests. With more inspection, it is revealed that the locations of these two peaks are near to the positions of the reactant gases manifolds in the bipolar plates. These manifolds were not considered in the numerical model. Hence, inserting reactants manifolds in these locations causes these two temperature peaks be vanished and the temperature becomes more uniform along horizontal edges of the stack, as seen from experimental results. Temperature profiles along two vertical half-edges of the bipolar plate (one close to the inlet coolant manifold and the other close to the exit coolant manifold) are shown in Fig. 14b. Here, there is also a good agreement between the simulation and the experimental results. As expected, the temperature in any point on the edge which is near to the exit manifold is higher than that of its corresponding point on the edge near to the inlet manifold. This is due to the fact that the coolant temperature at the exit region of cooling flow field is higher than that of the inlet region; therefore, temperature of the bipolar plate at this region should be higher in order to maintain constant heat flux.

5. Conclusion

Design of cooling flow field as well as thermal management subsystem of a 5 kW PEM fuel cell system were investigated in this paper. The number of parallel channels in the parallel serpentine flow field was selected as the design parameter and its optimum value was obtained by compromising between the minimum pressure drop of coolant across the flow field and the maximum temperature uniformity within the bipolar plate criteria. Coolant flow rate was also selected as the design parameter of the thermal management subsystem of the 5 kW PEM fuel cell system. The flow rate of 24 LPM was determined as the optimum coolant flow rate by compromising between maximum temperature uniformity within the bipolar plates of the stack and the minimum power consumption of the coolant circulation pump criteria. Larger coolant flow rate causes more uniform temperature distribution while lower flow rate leads to lower pressure drop and parasitic losses. Numerical simulation results were verified by comparing experimentally measured temperature profiles along the vertical and horizontal edges of the bipolar plates with those obtained by the numerical simulation. In addition, the following results were obtained:

- Inlet and outlet manifolds of reactant gases have an influence on the temperature distribution within the bipolar plates. So, uniformity of temperature distribution is one of the important factors that should be considered in the design phase of reactants manifolds.
- Free convection from stack faces has a negligible role on heat removal and can be ignored in the numerical simulation.

Acknowledgement

The authors would like to acknowledge the financial support of Renewable Energy Organization of Iran (SUNA).

References

[1] S.G. Kandlikar, Z. Lu, Appl. Therm. Eng. 29 (2009) 1276–1280.
[2] M.J. Lampinen, M. Fomino, J. Electrochem. Soc. 140 (1993) 3537–3546.
[3] J. Ramousse, O. Lottin, S. Didierjean, D. Maillet, J. Power Sources 192 (2009) 435–441.
[4] J. Larminie, A. Dicks, Fuel Cell Systems Explained, second ed., John Wiley & Sons, 2003.
[5] A. Faghri, Z. Guo, Int. J. Heat Mass Transfer 48 (2005) 3891–3920.
[6] Y. Shan, S.-Y. Choe, S.-H. Choi, J. Power Sources 165 (2007) 196–209.
[7] Y. Zong, B. Zhou, A. Sobiesiak, J. Power Sources 161 (2006) 143–159.
[8] C. Bao, M. Ouyang, B. Yi, Int. J. Hydrogen Energy 31 (2006) 1040–1057.
[9] L. Dumercy, R. Glises, H. Louahlia-Gualous, J.M. Kauffmann, J. Power Sources 156 (2006) 78–84.
[10] F.C. Chen, Z. Gao, R.O. Loutfy, M. Hecht, Fuel Cells 3 (2003) 181–188.
[11] J. Musser, C.Y. Wang, Proceedings of NHTC'00, 34th National Heat Transfer Conference, Pittsburgh, 2000.
[12] Y. Zhang, M. Ouyang, Q. Lu, J. Luo, X. Li, Appl. Therm. Eng. 24 (2004) 501–513.
[13] K.P. Adzakpa, J. Ramousse, Y. Dubé, H. Akremi, K. Agbossou, M. Dostie, A. Poulin, M. Fournier, J. Power Sources 179 (2008) 164–176.
[14] S. Yu, D. Jung, Renew. Energy 33 (2008) 2540–2548.
[15] Z. Qi, A. Kaufman, J. Power Sources 111 (2002) 181–184.
[16] F.P. Incropera, D.P. DeWitt, Fundamentals of Heat and Mass Transfer, fourth ed., John Wiley & Sons., Inc., New York, 1996.